Investigation of N-Terminal Domain Charged Residues on the Assembly and Stability of HIV-1 CA†

Chanel C. Douglas, Dennis Thomas,§ Jason Lanman,|| and Peter E. Prevelige, Jr.*

Department of Microbiology, University of Alabama at Birmingham, Birmingham, Alabama 35294-2170

Received April 1, 2004; Revised Manuscript Received May 13, 2004

ABSTRACT: The human immunodeficiency virus type 1 (HIV-1) capsid protein (CA) plays a crucial role in both assembly and maturation of the virion as well as viral infectivity. Previous in vivo experiments generated two N-terminal domain charge change mutants (E45A and E128A/R132A) that showed an increase in stability of the viral core. This increase in core stability resulted in decreased infectivity, suggesting the need for a delicate balance of favorable and unfavorable interactions to both allow assembly and facilitate uncoating following infection. Purified CA protein can be triggered to assemble into tubelike structures through the use of a high salt buffer system. The requirement for high salt suggests the need to overcome charge/charge repulsion between subunits. The mutations mentioned above lie within a highly charged region of the N-terminal domain of CA, away from any of the proposed protein/protein interaction sites. We constructed a number of charge mutants in this region (E45A, E45K, E128A, R132A, E128A/R132A, K131A, and K131E) and evaluated their effect on protein stability in addition to their effect on the rate of CA assembly. We find that the mutations alter the rate of assembly of CA without significantly changing the stability of the CA monomer. The changes in rate for the mutants studied are found to be due to varying degrees of electrostatic repulsion between the subunits of each mutant.

Retroviruses such as human immunodeficiency virus type 1 assemble through the polymerization of the Gag and Gag−Pol polyproteins. The Gag protein of HIV-1[1] is a 55 kDa protein that consists of the structural domains matrix (MA), capsid (CA), p2, nucleocapsid (NC), p1, and p6 (in that order) (*1*−*5*). A −1 ribosomal frame shift results in the Gag−Pol polyprotein, which adds the enzymatic proteins that include protease (PR), reverse transcriptase (RT), and integrase (IN) (*1*, *2*, *6*). The Gag and Gag−Pol polyproteins together with the Env protein comprise all of the structural and enzymatic proteins needed for viral infectivity. The polyproteins assemble under the plasma membrane and upon budding are found, in the immature virion, radially arranged with the N-myristoylated terminus of the matrix domain proximal to the viral envelope (*7*, *8*). During maturation, the Gag and Gag−Pol polyproteins are cleaved, releasing the structural proteins (MA, CA, and NC) that are then free to form new intersubunit interactions (*1*, *2*). In fact, cleavage results in a profound morphological change in which the capsid and nucleocapsid proteins collapse to form a conical core (*1*, *2*). Formation of the mature viral core is a critical step in the virus life cycle; mutations that block maturation or result in the formation of cores with aberrant morphology inhibit infectivity (*9*−*15*), in at least some cases by blocking the initiation of reverse transcription (*13*). Stability of the cores is also a factor in infectivity (*16*). Cores that are too stable may resist the process of uncoating and prevent release of the viral genome. Recent real-time observation of virus movement intracellularly showed the migration of intact cores along microtubules toward the nuclear envelope (*17*). If uncoating cannot take place before the core reaches the nuclear envelope, the complex may be perceived by the cell as being an aggregate of misfolded protein, and the core may be rerouted, ultimately to a lysosome (*18*).

A number of studies have demonstrated the ability of the capsid protein to polymerize into dimers, larger oligomers, and eventually tubular polymers (*14*, *19*−*21*). The presence of small amounts of cones similar in shape and size to viral cores has been described in some of these preparations (*22*, *23*). This indicates that in vitro assembled capsid polymers are capable of forming bonding interactions similar to those found in the virion. The in vitro assembly protocols for CA induce polymerization by utilizing high salt concentrations suggesting the need to overcome charge/charge repulsion between subunits (*14*, *19*−*21*).

High-resolution structures of CA obtained by X-ray crystallography and NMR demonstrate that it is composed of structurally distinct N- and C-terminal domains (*24*−*28*). Merging the crystal structure into cryoEM-based reconstructions of in vitro tubes suggested that the N-terminal domain

† This work was supported by NIH Grants AI44626 (P.E.P.). C.C.D. and J.L. were supported by NIH Training Grants AI007150 and CA09467, respectively. Support was also provided by NIH CFAR Core Grant P30AI27767 in construction of the mutants.

* Corresponding author. Phone: (205) 975-5327. Fax: (205) 975-5479. E-mail: prevelig@uab.edu.

§ Present address: Department of Biology, Rosenstiel Basic Medical Sciences Research Center, Brandeis University, Waltham, MA 02454.

|| Present address: Department of Molecular Biology, The Scripps Research Institute, La Jolla, CA 92037.

[1] Abbreviations: WT, wild-type; CTD, C-terminal domain; NTD, N-terminal domain; CD, circular dichroism; HIV-1, Human Immunodeficiency Virus-1; CA, capsid; NMR, nuclear magnetic resonance; PCR, polymerase chain reaction; ESI-TOF, electron spray ionization-time-of-flight; SIVcpz, Simian Immunodeficiency Virus chimpanzee; EM, electron microscopy.

10.1021/bi049359g CCC: $27.50
Published on Web 07/24/2004

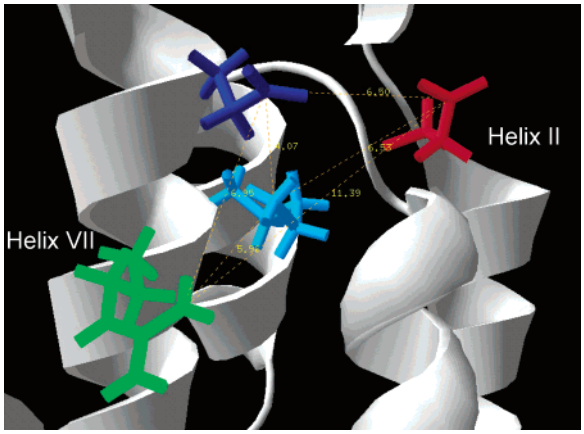

FIGURE 1: Structure of the highly charged region in the N-terminal domain of HIV-1 CA protein. Close-up view of the N-terminal domain structure as determined by NMR (PDB 1GWP) showing the amino acids mutated in this study. The distances between amino acids are also indicated. This figure was drawn with DeepView 3.7. E45—red, E128—blue, K131—cyan, and R132—green.

forms hexamers stabilized by NTD homotypic interactions, and the hexamers are tied together by CTD dimerization (*23*). While obtaining high-resolution structural information about the interactions driving capsid assembly has proven difficult, this model is well-supported by mutational and mass spectroscopic data both of which also provide evidence for an additional intersubunit NTD:CTD interaction (*29*−*31*).

It is known that the C-terminal domain dimer is stable in both low and high salt (*25*). This suggests that it is either the homotypic N-terminal domain interactions or the heterotypic N/C domain interactions that are salt sensitive. Additionally, mutagenesis studies have uncovered residues away from these sites of interaction that enhance the stability of the viral core and cause the virion to be less infectious (*16*). Two of these mutations are found in the N-terminal domain at positions E45 and E128/R132 and are located in helix 2 and helix 7, respectively. These mutations replaced charged residues with the neutral amino acid alanine, once again suggesting a role for charge/charge repulsion between subunits not only during assembly but during uncoating as well. To determine if the altered capsid stability was due to electrostatic or conformational effects, we generated a family of charge change mutants within this region (Figure 1) and evaluated their ability to stably fold and assemble.

MATERIALS AND METHODS

Protein Expression and Purification. A pET-based plasmid for expression of wild-type (WISP93-73) was obtained from W. Sundquist and transformed into *Escherichia coli* BL21-(DE3). Plasmids for expression of the mutant HIV-CA were obtained by PCR mutagenesis of the wild-type plasmid and verified by DNA sequencing. Wild-type (WT) and mutant capsid proteins were expressed and purified as previously described except where noted. The pH of the resuspension buffer for the mutants was increased from 8.0 to 8.5. The minimum percentage of ammonium sulfate used for efficient precipitation varied for each mutant ranging from 20 to 35%. The mutants were eluted from the Q-Sepharose (Amersham Biosciences) column at NaCl concentrations ranging from 70 to 90 mM. Most of the K131E protein was found to be irreversibly aggregated after the ammonium sulfate precipitation step; therefore, this step was eliminated from the purification protocol. Instead, the supernatant from the high-speed spin was applied both to an SP and to a Q-Sepharose column run in series. CA passed through the SP column, which retained other cellular proteins, and bound to the Q column. The protein was then eluted from the Q column independently. The eluted proteins were then dialyzed into 50 mM Na_2PO_4 buffer, pH 8.0. The mass of the each mutant protein as determined by ESI-TOF mass spectrometry was within 2 Da of the expected value. Purified protein solutions were stored frozen at −80 °C at ∼300−500 μM in 50 mM Na_2PO_4 buffer pH 8.0 until needed.

In Vitro Capsid Assembly. Purified wild-type and mutant capsid protein were assembled by rapid dilution into concentrated NaCl solutions at 20 °C to yield the desired final salt and protein concentration, and the course of the reaction was monitored by turbidity. For kinetic analysis, the reaction was rapidly mixed and placed into a 1-mm quartz cuvette. Unless otherwise noted, approximately 20 s elapsed between the time of the addition of salt and the first time point measured. The increase in optical density was monitored at 350 nm for 1 h as previously described (*32*), except where noted. The initial rate of assembly was approximated by fitting the early time points to a linear equation.

Determination of the Critical Concentration. To determine the fraction of unpolymerized protein present at equilibrium, assembly reactions were performed over a range of starting concentrations (20, 30, 40, 50, 60, and 70 μM for WT, E128A, R132A, and E128A/R132A; 10, 15, 20, 30, 40, and 50 μM for E45A; and 30, 40, 50, 60, 70, and 80 μM for K131A) and allowed to proceed to completion (1 h). The assembled polymers were collected by centrifugation at 14 000 rpm for 20 min in a microfuge. The supernatant was removed, and the pellets were resuspended in 400 μL of 50 mM Na_2PO_4 pH 8.0 with 3 M GuHCl included to dissociate the tubes and reduce scattering. The concentration of protein in supernatant or pellet was determined spectroscopically at 280 nm using an extinction coefficient of 33 460 M^{-1}. The amount of protein present in the supernatant fraction was used to determine the amount of unpolymerized protein in each sample.

Circular Dichroism. CD spectra of WT CA and all mutants were recorded on an AVIV model 620S at 20 °C in 50 mM Na_2HPO_4 pH 8.0 at concentrations ranging from 0.33 to 0.5 mg/mL. Readings were collected at 1 nm intervals from 195 to 260 nm with a 15 s averaging time. Actual concentrations were determined by collecting UV spectra at 280 nm of the sample measured, and the CD spectra were normalized according to the following equation: $[\theta] = (\theta\ 100M_r)/(clN_A)$. The recorded spectra in millidegrees of ellipticity (θ) were converted to mean residue ellipticity $[\theta]$ in deg cm^2 $dmol^{-1}$ by the equation, where c is the protein concentration in mg/mL, l is the path length in cm, M_r is the protein molecular weight, and N_A is the number of amino acids in the protein. Thermal melting curves were determined for all samples at a concentration of 1 μM in the same buffer using 1 cm path length cells. The temperature was increased in steps of 1.0 °C with a 12 s equilibration time over a nominal range of 25−90 °C. The actual temperature was recorded, and the observed range was typically ∼22−83 °C. Molar ellipticity readings were recorded at 218 nm using a 5 s averaging time and a bandwidth of 2.0 nm. The melting point for each

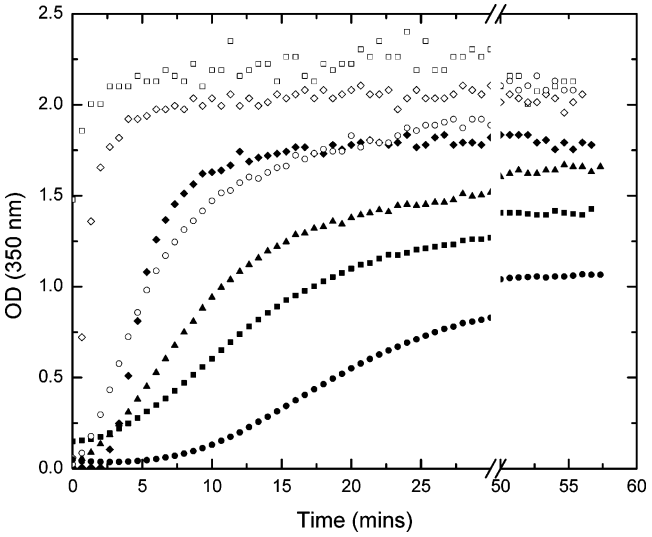

FIGURE 2: Assembly of wild-type and mutant CA proteins at 50 μM as followed by turbidity. CA protein was assembled at 50 μM at final NaCl concentration of 2.25 M. Symbols: WT (◆), E45A (□), E45K (▲), E128A (◇), R132A (■), E128A/R132A (○), and K131A (●). Every other data point is shown for clarity.

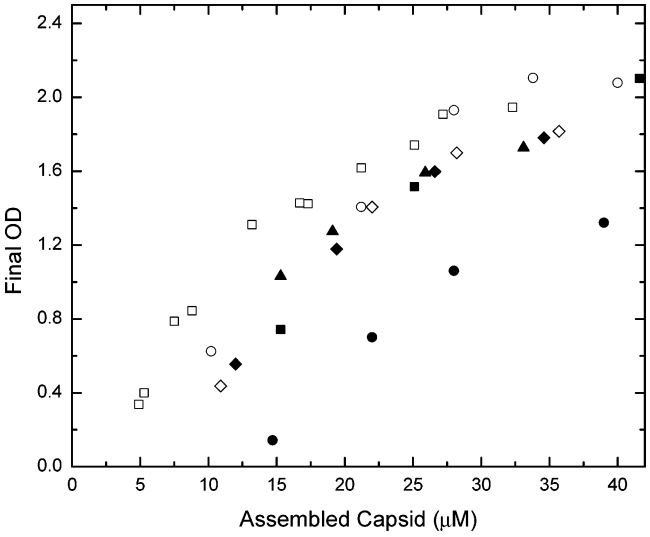

FIGURE 3: Dependence of the turbidity on the concentration of polymerized capsid. Final turbidity versus the concentration of polymerized protein after 1 h of assembly at 2.25 M salt and varying initial protein concentrations. The polymerized protein was pelleted, and the concentration in the pellet was determined by resuspension in 3 M GuHCl followed by absorbance spectroscopy. Symbols: WT (◆), E45A (□), E45K (▲), E128A (◇), R132A (■), E128A/R132A (○), and K131A (●).

mutant was determined by calculating the first derivative of the melting curve (ellipticity vs temperature) to determine the inflection point of the transition.

Sedimentation Equilibrium. Sedimentation equilibrium experiments on wild-type and mutant CA protein were performed at protein concentrations of 5.6, 9.8, and 15.8 μM in 50 mM sodium phosphate (pH 8.0) at 20 °C. Data were obtained using a Beckman Optima XL-A analytical ultracentrifuge at rotor speeds of 15 000, 20 000, and 25 000 rpm using an An-60 Ti rotor equipped with Epon charcoal-filled 12 mm six-channel centerpieces in cells with quartz windows. The absorbance was monitored at 280 nm, and 10 scans were averaged. The partial specific volume was determined using the public domain software program SEDNTERP (http://www.rasmb.bbri.org/) developed by Hayes, Laue, and Philo (*33*). Solution densities were obtained from standard tables. The equilibrium data from all nine experiments were fit globally to different models to determine the stoichiometry and association constant that best fit the data (*34*).

RESULTS

Change in Charge State Has Effect on Rate of Assembly. Previous in vivo studies have demonstrated that the N-terminal domain mutations E45A and E128A/R132A result in an increase in the stability of the viral core and a decrease in viral infectivity. Should the increased stability result from decreased intersubunit repulsion, the assembly reaction might take place faster because the decreased repulsion could facilitate the close approach of the subunits required for docking. Therefore, to determine if the increase in stability of these two mutants correlated with an increase in the rate of assembly, the assembly kinetics of purified capsid protein mutants were followed turbidimetrically (Figure 2) at 50 μM protein concentration. The initial rate of assembly was then estimated from the slope of the linear part of the curve (typically <10 min). The E45A mutant, which in the in vivo studies is 29-fold less infectious (*16*, *29*), assembled 33 times faster than wild-type, whereas E45K, a charge reversal mutant, assembled slower (40% of WT), suggesting that the presence of charged residues in this location affects association. The double mutant E128A/R132A displayed kinetic properties similar to wild-type, although in vivo it was 6.2-fold less infectious (*16*, *29*). To determine the relative contributions of E128A and R132A to the assembly kinetics, each mutation was examined individually. The E128A mutant assembled approximately twice as fast as wild-type, while R132A assembled at approximately half the rate of wild-type.

The three mutations (E45A, R128A, and E132A) studied previously lie within a 12 Å (most within 7 Å) radius of each other in the NMR structure of CA (Figure 1), a distance compatible with the formation of long-range ion pairs. One other charged residue, K131, lies in the middle of this cluster. To evaluate the role of K131 in assembly, this residue was mutated to the opposing and neutral charges and the effect studied. Both K131E (data not shown) and K131A assembled slower (10−20-fold less) than wild-type. These results suggest the need for charge balance in this region, a suggestion supported by the fact that sequence comparison between HIV-1 strains shows conservation of the charges at all positions in this cluster. The only exception to this is E128, which had two nonconservative changes out of the 380 clones strains available in the Los Alamos HIV-1/SIVcpz database.

To determine whether the turbidity was proportional to the amount of polymerized CA, assembly reactions were initiated at different initial CA concentrations and allowed to go to completion. The polymerized CA was separated from the unpolymerized subunits by centrifugation, and the maximum turbidity observed for each initial concentration was plotted against the amount of polymerized CA found in the pellet fraction after centrifugation (Figure 3). For all the mutants, the observed turbidity was directly proportional to the amount of protein polymerized. In the case of E45A and K131A, the absolute amount of turbidity per unit CA was different from the wild-type and the other mutants, suggesting

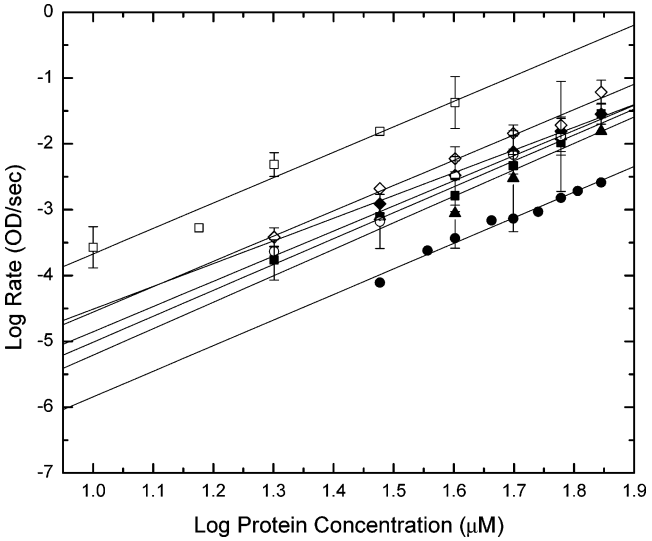

FIGURE 4: Dependence of the assembly rate on the protein concentration. CA protein was assembled at various protein concentrations at 2.25 M NaCl. The logs of the rate are plotted vs the log of the protein concentration, and the resulting curves are fit to a least-squares linear equation. Error bars represent the standard deviation of the measurements. The slope of the curves are similar to wild-type for each mutant studied, suggesting that the rate-limiting step is made up of the same number of subunits for each mutant. Symbols: WT (◆), E45A (□), E45K (▲), E128A (◇), R132A (■), E128A/R132A (○), and K131A (●).

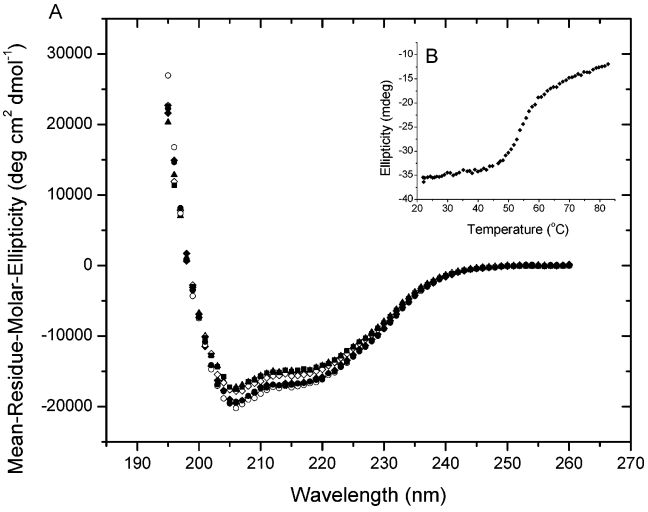

FIGURE 5: Circular dichroism spectra for wild-type and mutants and representative trace of thermal melting. (A) CD spectra of WT capsid and all mutants were recorded at 25 °C in 50 mM Na_2HPO_4 pH 8.0 at protein concentrations ranging from 0.33 to 0.5 mg/mL. The raw spectra were corrected for the concentration differences and background contributed by buffer and normalized using the equation found in the Materials and Methods. The CD spectra are similar and showed no clear differences in secondary structure under these conditions. (B) Shows the CD signal at 218 nm as the temperature is raised for wild-type capsid protein. The melting point was determined by taking the first derivative of the melting curve. The transition temperature for each mutant is found in Table 1. Symbols are the same as Figure 4.

that the structures of the final products might be different. While all the mutants examined by thin section electron microscopy (E45A, E45K, E128A, R132A, and E128A/R132A) formed tubes, the E45A mutant formed substantially shorter tubes (data not shown).

If the mutants alter the rate of subunit addition through charge/charge repulsion, the assembly pathway should remain unchanged. A way to measure this would be to look at the dependence of the rate of assembly on protein concentration, which provides an indication of the number of molecules involved in the rate-determining step. Therefore, assembly reactions were performed with each mutant over a range of concentrations, and the log of the rate of the reaction was plotted versus the log of the initial protein concentrations to derive the order of the reaction (Figure 4). The slopes of the mutants are nearly parallel to that of wild-type, suggesting that for all of the mutants, the change in the rate of assembly can be attributed to a change in the rate of subunit association as opposed to a change in the pathway of assembly.

Change in Rate Is Not Due to Altered Folding or Stability. It is possible that the increases or decreases in the rate of assembly are due to changes in the conformation or stability of the protein subunit. Therefore, to determine if the mutations were causing changes in the structure of the capsid protein, the CD spectra of each mutant was obtained at low protein concentration where the majority of the capsid protein is monomeric (Figure 5A). The CD spectra of the mutants were identical, within experimental error, to that of the wild-type, suggesting very little (if any) perturbation of the secondary structure. To measure the stability of the capsid monomer, the thermal stability of each protein was monitored by melting the protein and recording the molar ellipticity at 218 nm (Table 1). The melting point was determined by taking the first derivative of the melting curve (Figure 5B). With the exception of K131E, the mutants have the same or only slightly lower thermal melting transitions, suggesting that the mutations have minimal effects on the stability of the monomer. In the case of K131E, the lowered T_m reveals a second thermal transition. Detailed calorimetric studies of the melting of wild-type CA demonstrated independent melting of the N- and C-terminal domains (Protesevich et al., manuscript in preparation). The C-terminal domain melts at a slightly higher temperature than the N-terminal domain. The K131E mutation destabilized the N-terminal domain, revealing the underlying C-terminal domain melting transition.

Table 1

mutant	melting point (°C)[a]	second point	K_d (μM)[b]
wild-type	54		16
E45A	52		25
E45K	52	64	12
E128A	54		18
R132A	53		18
E128A/R132A	54		31
K131A	53		27
K131E	45	62	25

[a] The melting point was determined by taking the first derivative of the molar ellipticity melting curve recorded at 218 nm (Figure 5B). [b] The dissociation constant (K_d) of each protein was determined using the sedimentation equilibrium of the mutants at protein concentrations of 5.6, 9.8, and 15.8 μM and for three speeds, 15 000, 20 000, and 25 000 rpm at 20 °C. The absorbance spectra were recorded at 280 nm, and the data were analyzed using an Origin 4.1/Beckman analysis program.

Change in Rate Is Not Due to Altered Dimerization. The ability of the C-terminal domain of CA to dimerize is critical for capsid assembly. C-Terminal domain mutants, such as W184A/M185A, which cannot dimerize, cannot assemble (*32*). To ensure that the N-terminal domain charge change

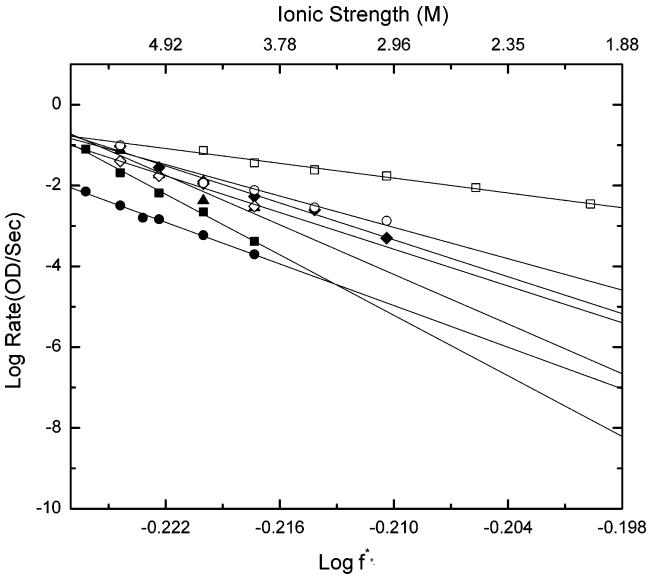

FIGURE 6: Dependence of the assembly rate on the salt concentration. CA protein was assembled at 50 μM at various NaCl concentrations. The log of the rate was plotted vs the log $f^*_{\times b1}$, where $f^*_{\times b1}$ is the electrostatic component of the mean rational activity coefficient of the ions (*35*). The resulting data points were fit to a least-squares linear equation. At high ionic strength, the lines converge as charge/ charge shielding becomes complete. Symbols: WT (◆), E45A (□), E45K (▲), E128A (◇), R132A (■), E128A/R132A (○), and K131A (●).

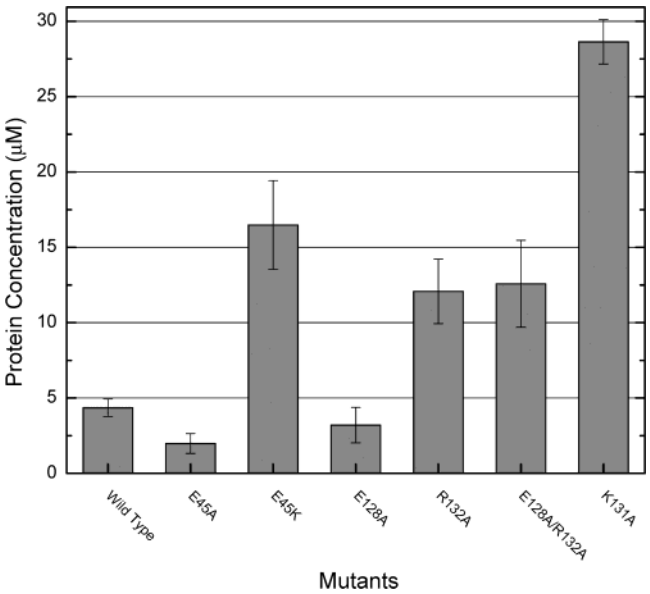

FIGURE 7: Critical concentration for the mutants at 2.25 M NaCl. CA was induced to assemble at concentrations ranging from 10 to 80 μM at 2.25M NaCl and allowed to assemble for 1 h. The polymerized and unpolymerized material were separated by centrifugation, and the concentrations of both were determined at 280 nm with an extinction coefficient of 33460 M^{-1}. The values shown in the bar graph depict the concentration of unassembled protein found in the supernatant fraction. The average of six to 10 concentrations/samples were used to obtained the values shown. The average sample lost was 13%.

mutations did not affect dimerization, the K_d of each mutant was determined using sedimentation equilibrium at three protein concentrations, 5.6, 9.8, and 15.8 μM, and for three rotor speeds, 15 000, 20 000, and 25 000 rpm at 20 °C as previously done for wild-type. The K_d of all the mutants (Table 1) was within experimental error, indicating similar dimerization abilities.

Magnitude of the Rate Differences Depend on the Salt Concentration. Should the effect of the mutations on assembly rate be strictly electrostatic, the effect of salt on the rate of assembly will vary for each mutant in proportion to the degree of shielding required for effective assembly. At infinite salt concentration, the rates of all the mutants should converge as charge shielding completely masks the charge/charge repulsion (*35*). To test this, the dependence of the rate on salt concentration was determined. The mutant capsid proteins were assembled at 50 μM at various salt concentrations ranging from 1 to 3 M depending on the mutant. The rate was then determined, and the log was plotted against the log of the initial salt concentration. From Figure 6, it can be seen that slopes of the resulting linear fits differ among the mutants, suggesting that the dependence of the rate of assembly on the salt concentration (i.e., the charge screening capability) is different for each mutant studied. The rates of assembly for the mutants converge at high salt concentrations, as expected. However, one mutant, K131A, appears to have the same dependence on salt concentration as wild-type as the slope runs parallel to wild-type, which suggests the change in rate may not be solely due to electrostatic effects for this mutant. The extent of polymerization as monitored by the final amount of turbidity was found to be salt independent at later times, as previously demonstrated (data not shown) (*32*).

Energetics of Assembly Depend on the Charge. In performing the experiment to determine the correspondence between turbidity and amount of protein polymerized, we noticed that the amount of protein in the supernatant was relatively constant. This represents the critical concentration of the reaction. The critical concentration for polymerization reflects the equilibrium between subunit addition and dissociation and thus serves as an indication of the energetics of intersubunit interactions (*36*−*39*).

To determine if the mutations altered the critical concentration, we measured the amount of unpolymerized protein for each mutant across a range of concentrations (Figure 7). The data demonstrate that the mutants do alter the critical concentration, and the alterations correspond to their observed effects on assembly; mutants with lower critical concentration show faster assembly. The alternative model, in which the mutations cause a slight folding defect resulting in a fraction of unassociable protein, would result in a constant percentage of unpolymerized protein rather than a constant concentration. This was not observed.

DISCUSSION

We have previously reported the development of a rapid dilution-induced technique for CA assembly (*32*). This technique has proven to be useful for the evaluation of the effects of solvent conditions, protein concentration, and mutations on CA assembly. Here, we extend the use of this technique to analyze the effect of N-terminal domain charge change mutations on CA assembly. The mutations E45A and E128A/R132A have been previously reported to result in an increase in core stability (*16*). Thermodynamically, an increase in stability of a complex is due to an increase in the favorability of the interactions in the complex. Such an increase could lead to an enhancement in the rate of formation of the complex. In the case of E45A, we see a

corresponding increase in the rate of assembly. For E128A/R132A, the observed increase in stability does not result in a corresponding increase in the overall rate of assembly. This seems to arise from a balancing of two opposite effects as can be seen from the analysis of the mutations individually. The E128A mutation results in faster assembly kinetics, while the R132A mutation results in slower assembly kinetics. For the mutants studied, there is a correlation between the critical concentration and the kinetics of assembly. The exception to this is the E128A/R132A mutant, which assembles at a rate similar to wild-type but has a higher critical concentration. This concentration is in fact similar to one of its single mutants, R132A. The other three mutants studied, E45K, K131A, and K131E, had slower assembly kinetics. K131E was difficult to purify and study, limiting the data obtained, as this charge change destabilized the protein. For E45K and K131A, the decrease in assembly kinetics might be due to increased electrostatic repulsion between the subunits as suggested by the critical concentration. Another possibility for the higher critical concentration for these mutants may be difficulty in a nucleation-like step. We have observed that the assembly of K131A is greatly enhanced by the addition of E45A, which may serve to nucleate the assembly reaction (data not shown).

There are three protein−protein interactions within CA that are required to stabilize the core. These are the C-terminal domain dimerization mediated by hydrophobic packing of CA helix IX (*25*, *27*), the N-terminal domain homotypic interactions mediated by helices I and II (*23*), and an N- to C-domain intersubunit interaction mediated by the loop between helices III and IV and the base of helix IV in the NTD and helices VIII and IX in the CTD (*30*). As expected, in general, mutations at residues within these interfaces prevent capsid assembly. The mutants presented here do not lie within any of these regions but rather within the core of the N-domain. However, they affect the kinetics and stability of at least two of these interactions without significantly changing the conformation or stability of the monomeric protein subunit itself. These charged residues are highly conserved in both HIV-1 and SIVcpz. This suggests that the HIV-1 CA may have evolved to be a protein primed for dissociation. In fact, the association constants for each of these interactions is relatively weak. Despite the importance of the homotypic N-terminal domain interactions in the structure of the core, they are unable to form independently of the other stabilizing CA interactions. The N-domain carrying the mutation (E45A), which forms a more stable core, was also unable to oligomerize in solution independently of the C-terminal domain (data not shown). The C-terminal domain dimer is relatively weak with a K_d of 18 μM (*25*). Interestingly, point mutation in the C-terminal domain such as Ser-178, Glu-180, Glu-187, and Gln-192 leads to more stable dimers (*40*). This suggests that the overall stability of the CA domain of HIV-1 is balanced to allow both assembly and disassembly.

An emerging theme is that charge/charge repulsion plays a significant role in HIV-1 assembly and disassembly. Scanning alanine mutagenesis of CA uncovered many charged residues that when neutralized had normal particle production but reduced infectivity (*29*). Additionally, replacing neutral residues with charged residues resulted in reduced particle production and no infectivity (*14*). In the context of the virion, assembly of the capsid protein takes place in two stages. The first involves the association of the Gag polyprotein to form an immature virion, while the second involves cleavage of the Gag protein to its constituent structural domains and the condensation of the capsid protein to form the central conical core (*1*−*5*, *41*). Assembly of the virion requires a loss of entropy, which must be compensated by favorable interactions. There are multiple sites of interaction dispersed throughout the Gag polyprotein that can help promote capsid assembly. The N-terminal matrix (MA) domain is myristylated (*42*, *43*). The myristyl group inserts into the cell membrane increasing the effective concentration of the Gag polyprotein and reduces assembly to a two-dimension diffusion problem. The MA domain itself is capable of forming trimeric interactions (*43*−*45*). The NC-domain binds the viral RNA tightly through the action of charge clusters and zinc fingers (*42*). Multiple Gag proteins bind a single RNA molecule, once again providing a mechanism for increasing the concentration and decreasing the entropic penalty of assembly. Mutations in NC, which interfere with RNA binding, have a deleterious effect on virus assembly. Collectively, these interactions, all of which occur in a single polypeptide chain, are sufficient to overcome both the entropic loss as well as the charge/charge repulsion evident in the CA N-terminal domain.

Having assembled a capsid using the intact Gag polyprotein proteolytic cleavage during maturation then liberates CA, which collapses to form a conical core (*1*, *2*, *4*). Core formation is likely promoted by the high concentration of CA present in the virion, which has been estimated to be in the millimolar range (*41*). Fusion of the virion with the host cell results in the membrane being stripped away and the naked core entering the cytoplasm. At this point, the concentration of CA drops significantly, and uncoating could be facilitated by electrostatic repulsion between the subunits. Core stability has been shown to play an important role in infectivity, but the precise sequence and timing of initiation of reverse transcription, core dissociation, and nuclear transport of the preintegration complex remains a mystery.

ACKNOWLEDGMENT

We are grateful to Mike Jablonsky for assistance with CD and John Rodgers for assistance with the analytical ultracentrifuge.

REFERENCES

1. Freed, E. O. (1998) HIV-1 gag proteins: diverse functions in the virus life cycle, *Virology 251*, 1−15.
2. Hunter, E. (1994) Macromolecular interactions in the assembly of HIV and other retroviruses, *Semin. Virol. 5*, 71−83.
3. Mervis, R. J., Ahmad, N., Lillehoj, E. P., Raum, M. G., Salazar, F. H., Chan, H. W., and Venkatesan, S. (1988) The gag gene products of Human Immunodeficiency Virus type 1: alignment within the gag open reading frame, identification of posttranslational modifications, and evidence for alternative gag precursors, *J. Virol. 62*, 3993−4002.
4. Turner, B. G., and Summers, M. F. (1999) Structural biology of HIV1, *J. Mol. Biol. 285*, 1−32.
5. Nermut, M. V., and Hockley, D. J. (1996) Comparative morphology and structural classification of retroviruses, *Curr. Topics Microbiol. Immunol. 214*, 1−24.
6. Jacks, T., Power, M. D., Masiarz, F. R., Luciw, P. A., Barr, P. J., and Varmus, H. E. (1988) Characterization of ribosomal frameshifting in HIV-1 gag-pol expression, *Nature 331*, 280−283.

7. Fuller, S. D., Wilk, T., Gowen, B. E., Krausslich, H. G., and Vogt, V. M. (1997) Cryoelectron microscopy reveals ordered domains in the immature HIV-1 particle, *Curr. Biol. 7*, 729−738.
8. Wilk, T., Gross, I., Gowen, B. E., Rutten, T., de Haas, F., Welker, R., Krausslich, H. G., Boulanger, P., and Fuller, S. D. (2001) Organization of immature human immunodeficiency virus type 1, *J. Virol. 75*, 759−771.
9. Dorfman, T., Bukovsky, A., Ohagen, A., Hoglund, S., and Gottlinger, H. (1994) Functional domains of the capsid protein of human immunodeficiency virus type 1, *J. Virol. 68*, 8180−8187.
10. Fitzon, T., Leschonsky, B., Bieler, K., Paulus, C., Schroder, J., Wolf, H., and Wagner, R. (2000) Proline Residues in the HIV-1 NH2-Terminal Capsid Domain: Structure Determinants for Proper Core Assembly and Subsequent Steps of Early Replication, *Virology 268*, 294−307.
11. Reicin, A., Paik, S., Berkowitz, R., Luban, J., Lowy, I., and Goff, S. (1995) Linker insertion mutations in the human immunodeficiency virus type 1 gag gene: effects on virion particle assembly, release, and infectivity, *J. Virol. 69*, 642−650.
12. Reicin, A., Ohagen, A., Yin, L., Hoglund, S., and Goff, S. (1996) The role of Gag in human immunodeficiency virus type 1 virion morphogenesis and early steps of the viral life cycle, *J. Virol. 70*, 8645−8652.
13. Tang, S., Murakami, T., Agresta, B. E., Campbell, S., Freed, E. O., and Levin, J. G. (2001) Human Immunodeficiency Virus Type 1 N-Terminal Capsid Mutants that Exhibit Aberrant Core Morphology and Are Blocked in Initiation of Reverse Transcription in Infected Cells, *J. Virol. 75*, 9357−9366.
14. von Schwedler, U. K., Stemmler, T. L., Klishko, V. Y., Li, S., Albertine, K. H., Davis, D. R., and Sundquist, W. I. (1998) Proteolytic refolding of the HIV-1 capsid protein amino-terminus facilitates viral core assembly, *EMBO J. 17*, 1555−1568.
15. Wang, C., and Barklis, E. (1993) Assembly, processing, and infectivity of human immunodeficiency virus type 1 gag mutants, *J. Virol. 67*, 4264−4273.
16. Forshey, B. M., von Schwedler, U., Sundquist, W. I., and Aiken, C. (2002) Formation of a human immunodeficiency virus type 1 core of optimal stability is crucial for viral replication, *J. Virol. 76*, 5667−5677.
17. McDonald, D., Vodicka, M. A., Lucero, G., Svitkina, T. M., Borisy, G. G., Emerman, M., and Hope, T. J. (2002) Visualization of the intracellular behavior of HIV in living cells, *J. Cell Biol. 159*, 441−452.
18. Sodeik, B. (2002) Unchain my heart, baby let me go—the entry and intracellular transport of HIV, *J. Cell Biol. 159*, 393−395.
19. Campbell, S., and Vogt, V. (1995) Self-assembly in vitro of purified CA-NC proteins from Rous sarcoma virus and human immunodeficiency virus type 1, *J. Virol. 69*, 6487−6497.
20. Ehrlich, L., Agresta, B., and Carter, C. (1992) Assembly of recombinant human immunodeficiency virus type 1 capsid protein in vitro, *J. Virol. 66*, 4874−4883.
21. Gross, I., Hohenberg, H., and Krausslich, H. (1997) In vitro assembly properties of purified bacterially expressed capsid proteins of human immunodeficiency virus, *Eur. J. Biochem. 249*, 592−600.
22. Ganser, B. K., Li, S., Klishko, V. Y., Finch, J. T., and Sundquist, W. I. (1999) Assembly and Analysis of Conical Models for the HIV-1 Core, *Science 283*, 80−83.
23. Li, S., Hill, C. P., Sundquist, W. I., and Finch, J. T. (2000) Image reconstructions of helical assemblies of the HIV-1 CA protein, *Nature 407*, 409−413.
24. Gamble, T. R., Vajdos, F. F., Yoo, S., Worthylake, D. K., Houseweart, M., Sundquist, W. I., and Hill, C. P. (1996) Crystal structure of human cyclophilin A bound to the amino-terminal domain of HIV-1 capsid, *Cell 87*, 1285−1294.
25. Gamble, T. R., Yoo, S., Vajdos, F. F., von Schwedler, U. K., Worthylake, D. K., Wang, H., McCutcheon, J. P., Sundquist, W. I., and Hill, C. P. (1997) Structure of the carboxyl-terminal dimerization domain of the HIV-1 capsid protein, *Science 278*, 849−853.
26. Gitti, R. K., Lee, B. M., Walker, J., Summers, M. F., Yoo, S., and Sundquist, W. I. (1996) Structure of the Amino-Terminal Core Domain of the HIV-1 Capsid Protein, *Science 273*, 231−235.
27. Worthylake, D. K., Wang, H., Yoo, S., Sundquist, W. I., and Hill, C. P. (1999) Structures of the HIV-1 capsid protein dimerization domain at 2.6 Å resolution, *Acta Crystallogr. D55* (Pt 1), 85−92.
28. Tang, C., Ndassa, Y., and Summers, M. F. (2002) Structure of the N-terminal 283-residue fragment of the immature HIV-1 Gag polyprotein, *Nat. Struct. Biol. 9*, 537−543.
29. von Schwedler, U. K., Stray, K. M., Garrus, J. E., and Sundquist, W. I. (2003) Functional surfaces of the human immunodeficiency virus type 1 capsid protein, *J. Virol. 77*, 5439−5450.
30. Lanman, J., Lam, T. T., Barnes, S., Sakalian, M., Emmett, M. R., Marshall, A. G., and Prevelige, P. E., Jr. (2003) Identification of novel interactions in HIV-1 capsid protein assembly by high-resolution mass spectrometry, *J. Mol. Biol. 325*, 759−772.
31. Ganser-Pornillos, B. K., von Schwedler, U. K., Stray, K. M., Aiken, C., and Sundquist, W. I. (2004) Assembly properties of the human immunodeficiency virus type 1 CA protein, *J. Virol. 78*, 2545−2552.
32. Lanman, J., Sexton, J., Sakalian, M., and Prevelige, P. E., Jr. (2002) Kinetic Analysis of the Role of Intersubunit Interactions in Human Immunodeficiency Virus Type 1 Capsid Protein Assembly in Vitro, *J. Virol. 76*, 6900−6908.
33. Laue, T. M., Shah, B. D., Ridgeway, T. M., and Pelletier, S. L. (1992) in *Analytical ultracentrifugation in biochemistry and polymer science* (Al, S. E. H., Ed.) pp 90−125, The Royal Society of Chemistry, Cambridge, UK.
34. Johnson, M. L., Correia, J. J., Yphantis, D. A., and Halvorson, H. R. (1981) Analysis of data from the analytical ultracentrifuge by nonlinear least-squares techniques, *Biophys. J. 36*, 575−588.
35. Schreiber, G., and Fersht, A. R. (1996) Rapid, electrostatically assisted association of proteins, *Nat. Struct. Biol. 3*, 427−431.
36. Andreu, J. M., and Timasheff, S. N. (1986) The measurement of cooperative protein self-assembly by turbidity and other techniques, *Methods Enzymol. 130*, 47−59.
37. Harper, J. D., and Lansbury, P. T. (1997) Models of Amyloid Seeding in Alzheimer's Disease and Scrapie: Mechanistic Truths and Physiological Consequences of the Time-Dependent Solubility of Amyloid Proteins, *Ann. Rev. Biochem. 66*, 385−407.
38. Prevelige, P. E., Jr., Thomas, D., and King, J. (1993) Nucleation and growth phases in the polymerization of coat and scaffolding subunits into icosahedral procapsid shells, *Biophys. J. 64*, 824−835.
39. Oosawa, F., and Kasai, M. (1962) A theory of Linear and Helical Aggregations of Macromolecules, *J. Mol. Biol. 4*, 10−21.
40. del Alamo, M., Neira, J. L., and Mateu, M. G. (2003) Thermodynamic dissection of a low affinity protein−protein interface involved in human immunodeficiency virus assembly, *J. Biol. Chem. 278*, 27923−27929.
41. Briggs, J. A., Wilk, T., Welker, R., Krausslich, H. G., and Fuller, S. D. (2003) Structural organization of authentic, mature HIV-1 virions and cores, *EMBO. J. 22*, 1707−1715.
42. Coffin, J. M., Hughes, S. H., and Varmus, H. E. (1997) *Retroviruses*, Cold Spring Harbor Laboratory Press, Plainview, NY.
43. Tang, C., Loeliger, E., Luncsford, P., Kinde, I., Beckett, D., and Summers, M. F. (2004) Entropic switch regulates myristate exposure in the HIV-1 matrix protein, *Proc. Natl. Acad. Sci. U.S.A. 101*, 517−522.
44. Morikawa, Y., Zhang, W. H., Hockley, D. J., Nermut, M. V., and Jones, I. M. (1998) Detection of a trimeric human immunodeficiency virus type 1 gag intermediate is dependent on sequences in the matrix protein, p17, *J. Virol. 72*, 7659−7663.
45. Hill, C. P., Worthylake, D., Bancroft, D. P., Christensen, A. M., and Sundquist, W. I. (1996) Crystal structures of the trimeric human immunodeficiency virus type 1 matrix protein: Implications for membrane association and assembly, *PNAS 93*, 3099−3104.

BI049359G